

# SIGNAL PROCESSING FOR ORDER 10 PM ACCURACY DISPLACEMENT METROLOGY IN REAL-WORLD SCIENTIFIC APPLICATIONS

Peter G. Halverson<sup>(1)</sup>, Frank M Loya<sup>(2)</sup>

<sup>(1)</sup>Jet Propulsion Laboratory (JPL), California Institute of Technology,  
4800 Oak Grove Drive, Pasadena, CA 91109 U.S.A., Peter.G.Halverson@jpl.nasa.gov

<sup>(2)</sup>JPL, Frank.M.Loya@jpl.nasa.gov

## ABSTRACT

Projects such as the Space Interferometry Mission (SIM) [1] and Terrestrial Planet Finder (TPF) [2] rely heavily on sub-nanometer accuracy metrology systems to define their optical paths and geometries. The James Web Space Telescope (JWST) is using this metrology in a cryogenic dilatometer for characterizing material properties (thermal expansion, creep) of optical materials. For all these projects, a key issue has been the reliability and stability of the electronics that convert displacement metrology signals into real-time distance determinations. A particular concern is the behavior of the electronics in situations where laser heterodyne signals are weak or noisy and subject to abrupt Doppler shifts due to vibrations or the slewing of motorized optics. A second concern is the long-term (hours to days) stability of the distance measurements under conditions of drifting laser power and ambient temperature.

This paper describes heterodyne displacement metrology gauge signal processing methods that achieve satisfactory robustness against low signal strength and spurious signals, and good long-term stability. We have a proven displacement-measuring approach that is useful not only to space-optical projects at JPL, but also to the wider field of distance measurements.

## 1. INTRODUCTION

JPL's dimensional metrology challenges, typified by the efforts of the SIM metrology team [3],[4], TPF [5] and JWST [6] have forced the development of accurate phase measuring electronics to meet their metrology accuracy requirements which are listed in Table 1.

This paper discusses signal processing downstream of the interferometer in Fig. 1, starting with the photodiodes and continuing with preamps and integrated amplification, filtering and sine-to-square wave conversion devices called "post-amps" at JPL.

Since the laser wavelength  $\lambda$  is  $\sim 0.5$  or  $\sim 1$  micron and the accuracy  $\epsilon(L)$  needed is typically of order 10 picometers (pm), the heterodyne phases must be measured to  $2\epsilon(L)/\lambda \approx 2 \times 10^{-5}$  cycles.

Table 1. Metrology needs of various project testbeds and experiments. TPF and SIM testbed metrology experiences will influence flight implementations. JWST's metrology need is for materials evaluation purposes only and will not be used in flight.

	JWST dilatometer	TPF	SIM
Laser $\lambda$	532 nm	1.5 $\mu\text{m}$	1.3 $\mu\text{m}$
Linearity	<50 pm	$\sim 100$ pm	$\sim 10$ pm
Stability	<50 pm	$\sim 100$	$\sim 10$ pm
Time scale	Days	$\sim 1000$ s	hours

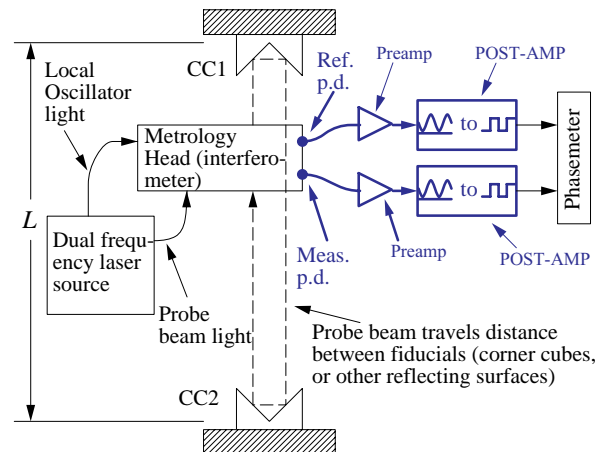


Fig 1. Context of the electronics discussed in this paper (bold). Heterodyne signals (2 kHz to 1 MHz) from the interferometer's photodiodes (p.d.) are amplified, filtered and converted to square waves by "post-amps". The phases of the square waves are measured by a phasemeter [7] and indicate  $L$ , the relative displacement of the fiducials in terms of the interferometer's laser wavelength.

## 2. LESSONS LEARNED

Our experience has shown that  $\epsilon(\phi) \approx 10^{-5}$  cycle accuracy phase measurements require care and attention to detail. Some of the obvious, and a few not-so-obvious lessons learned are summarized below:

1. *Shield the photodiode.* Many experiments have several cm long photodiode (p.d.) leads to

keep heat-producing preamplifiers away from the optics. To avoid RF pickup, it is essential that the leads and diode be shielded with conductive braid or foil. See Fig. 2.

2. *Keep the photodiode capacitance low.* This is an old story but is worth repeating: any capacitance to ground at the inverting input of the op-amp will hugely increase the noise at the op-amp output. We have kept it low by

- a. making our own shielded cables to the p.d.'s by inserting loosely twisted "wire-wrap" wire (thin wire with low surface area) into a loose braid,
- b. selecting low capacitance p.d.'s,
- c. reverse biasing the p.d.,

in decreasing order of importance. See Fig. 2.

3. *Distribute the gain.* To keep the number of parts down, experimenters tend to want to amplify the (often tiny) photodiode signals to practical levels (~1 volt) in one or two op-amp stages. This is a bad idea if the gain per op-amp is higher than 1000 V/V or 10000 V/A or if the gain  $\times F_{HET}$  approaches ~10% of the op-amp gain bandwidth product. To avoid parasitic oscillations and signal distortion, we are obliged to spread the gain across several op-amp circuits.

4. *Pay attention to op-amp slew rates.* An op-amp will begin to distort a sinusoid if the output voltage  $\times$  frequency approaches ~10% of the device's slew rate. Such distortion causes high sensitivity to signal strength variations thus degrading phase stability.

5. *Buffer the signals.* After the initial gain stage after the photodiode (the transimpedance amplifier) there is typically several meters of cable to get out of the vacuum tank and to the instrument racks. That first amplifier's performance will be degraded (often unstable) if it drives that load. Much better performance is achieved with dedicated buffers, which can also incorporate voltage gain.

6. *Use differential signals.* For better spurious signal rejection, long cable runs can greatly benefit from differential drivers and receivers. Suitable monolithic *analog* differential drivers have not been available, so we made our own as in Figs 3 and 4.

7. *Avoid multiple grounds, ground loops.* (Fig. 5) This is needed for low cross-talk between channels. Any alternate route for a heterodyne signal to return to the instrument rack other than via its signal cable is an invitation to transmitting or receiving signals from adjacent channels, causing cyclic error. For example, if the photodiode shield happens to touch the optical table, a large (~100 pm) cyclic error can be expected.

8. *Isolate your electronics.* This is an extension of the previous point. Eliminate all common grounds between the photodiodes and phasometers by running each photodiode, gain, filtering, and conversion to square waves processing chain on independent power supplies. Optically couple to the phasometers, so each channel is floating. (In practice, it is necessary to bleed excess charge, so the grounds may be connected to earth by 100 kOhm resistors.)

9. *Keep  $F_{HET}$ , the heterodyne frequency, low.* At high frequencies, cross talk increases, due to greater capacitive and inductive coupling. At high frequencies (above a few tens of kHz), the performance limits of op-amps are easily exceeded, resulting in distorted waveforms, and unexpected phase lags.

10. *Use wide bandpass filter frequencies.* A common mistake is to improve S.N.R. by installing a narrow bandpass around  $F_{HET}$ . This causes a large phase shift in the bandpass filter, which will vary with temperature. Keep the 3 dB points factors of >2 away from  $F_{HET}$ .

It should be noted that paying attention to the above points will also help eliminate "glitches", sudden integer cycle phase jumps caused by electrical noise (motors, lightning etc.).

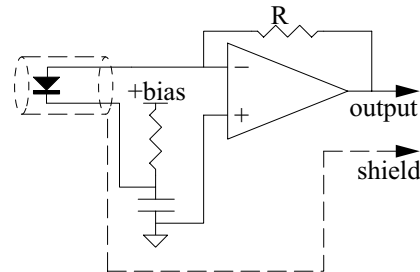


Fig. 2. Photodiode and transimpedance amplifier circuit with shielding. Note that the shield is distinct from circuit common.

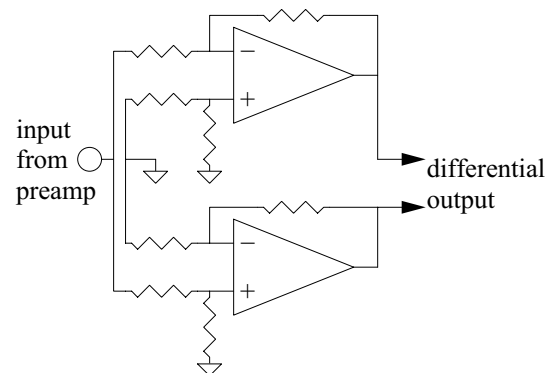


Fig. 3. Differential driver using two op-amps.

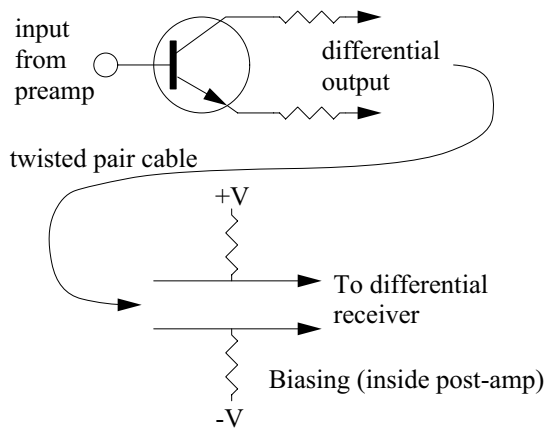


Fig 4. Differential driver using one transistor. This circuit [8] has very low heat dissipation, but requires bias at the receiving end of the cable.

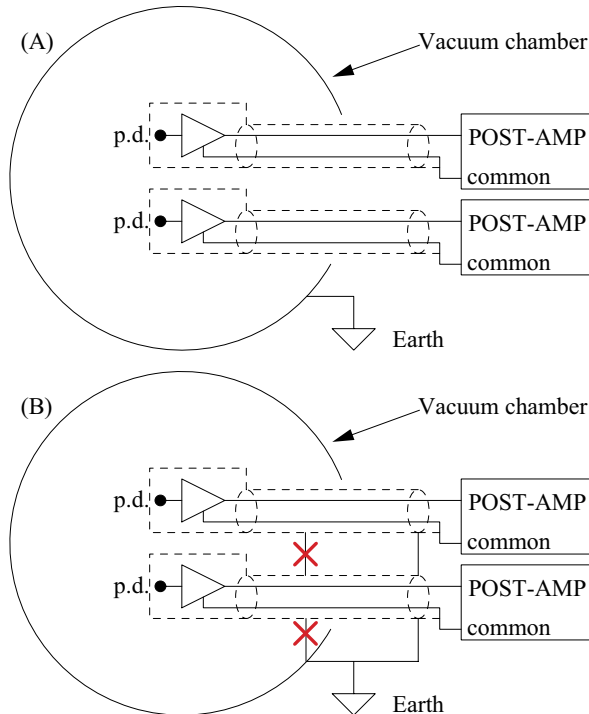


Fig 5. Shielding schemes, with shields shown in dashed lines. JPL experiments are typically in vacuum chambers, which are usually grounded. For low crosstalk and RF pickup, do “a”. Don’t do “b”. In “a”, the post-amp commons are shown disconnected, but if the output connections are not isolated, then the commons will link at the phasemeter. If the outputs *are* isolated (as in the new JWST/TPF post-amp), then it *might* be helpful to link the commons and possibly connect them to earth.

### 3. DRIFT ISSUES

Long-term stability of  $\sim 10^{-5}$  cycles is challenging. The major obstacles are signal-strength variation coupling

to phase error, and the thermal stability of the electronics.

(It might be noted that common-mode drift of all the channels, as would be caused by laser wavelength drift is not as much of a problem for current applications. We are concerned here with drift of a given channel relative to the others.)

#### 3.1 Laser signal strength variation and zero-crossing level.

Fig. 6 shows the conversion from sinusoid to square wave. At JPL, the device that performs this function is called a “Post-Amp” and we will use this term. (Post-amps also perform signal amplification and conditioning, so the name is reasonable.)

The amplitude of the sine wave input is proportional to the laser power and to the interferometric fringe contrast which, in real-world systems, can be expected to vary a few percent. (This is particularly true for fiber-optic coupled interferometers, where temperature changes affect polarization, affecting the fringe contrast.)

Since typical JPL testbeds have heterodyne signal amplitude drift  $R_A=5\%$ , if we want  $\epsilon(\phi)\approx 10^{-5}$  cycle stability, the amplitude-to-phase coupling  $d\phi/dR_A$  must be less than  $2 \times 10^{-4}$ .

The phase of the output square wave will not be affected by the input amplitude drift if

1. the input sine wave phase is itself constant and
2. the sine wave is undistorted (or at least symmetric) and
3. the sine wave and the comparator’s input offset voltages are both zero (or at least equal).

Requirements 1 and 2 will be approximately satisfied if low-distortion op-amps [9] are used upstream and are operated at low enough gain and amplitude to be far from their slew-rate and gain-bandwidth limitations. Example: if the op-amp GBWP=10 MHz and  $F_{HET}=100$  kHz, then the G must be  $< 100$ , preferably less. Similarly, if the slew-rate  $R=10V/\mu s$ , the gain must be  $< R/(2\pi F_{HET})=16$ . Evidently, the slew rate limitation is the more constraining.

Requirement 3 is problematic since all electronics experience some DC drift with temperature changes. Op-amp output drift can be eliminated by AC coupling, but comparator input offset, which is usually zeroed using an external potentiometer, cannot be eliminated. Quantitatively, a comparator offset voltage will cause a phase sensitivity

$$d\phi/dR_A = (1/\pi)(V_{\text{offset}}/V_{\text{pp}}) \quad (1)$$

in units of cycles, and where  $V_{\text{pp}}$  is the comparator input amplitude. Example: if  $V_{\text{pp}}=2$  Volts, and we require  $d\phi/dR_A < 2 \times 10^{-5}$ , then  $V_{\text{offset}}$  must stay within  $\pm 0.13$  mV. A typical comparator offset temperature coefficient is 0.01 mV/C, so for this example a 13 C range would be acceptable, ignoring all other effects.

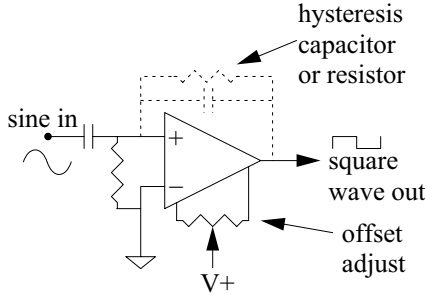


Fig. 6. Conversion of sinusoid to square wave. Dashed connections indicate optional hysteresis circuits.

The reader might suggest that using an automatic gain control (AGC) circuit would eliminate the amplitude variation problems just discussed, however it has proven difficult to construct an AGC circuit that doesn't introduce its own phase changes.

A practical obstacle in evaluating  $d\phi/dR_A$  is that amplitude modulated sine wave sources that are free of phase modulation at the  $10^{-6}$  level are not readily available. An approach we have found we can trust is shown in Fig. 7. Its advantage is that by using the same photodiode and electronics as in the final application, parasitic phase shifts are automatically taken into account.

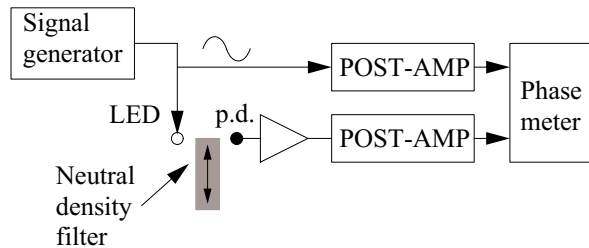


Fig. 7. Set up for testing amplitude-to-phase coupling. Signal generator set to  $F_{\text{HET}}$  drives LED and reference channel post-amp. Neutral density filter moved in/out of gap between LED and p.d., causes a varying amplitude but constant phase signal. The phase meter detects any spurious phase shift by comparing the two post-amp outputs.

### 3.2 Thermal stability of zero-crossing detector

Comparator offset drift  $\varepsilon(V_{\text{offset}})$  will, by itself introduce a phase drift

$$d\phi/dV_{\text{offset}} = 1/(\pi V_{\text{pp}}), \quad (2)$$

in cycles. Example:  $V_{\text{pp}}=2$  Volts, then for  $\varepsilon(\phi) \approx 10^{-5}$  cycles,  $\varepsilon(V_{\text{offset}})$  must be less than .063 mV. If the comparator offset temperature coefficient is 0.01 mV/C, then a 6.3 C range would be acceptable, ignoring all other effects.

The offset drift problem will be worsened by the addition of a hysteresis feedback resistor (Fig. 6, needed for a glitch-free square-wave output) which will couple comparator output drift (or power supply drift) to the input. This can be solved by using a capacitor instead of a resistor. The capacitor value must be carefully chosen to provide enough feedback to debounce the output, but not so much as to noticeably retard the output phase.

In practice, the current solution to the comparator drift problem is to stabilize the temperature, placing the electronics in a constant-temperature oven.

### 3.3 Thermal stability of bandpass filters

Another source of phase drift is the bandpass filters that are generally needed to remove RF pickup and noise from the photodiode signals. The circuit in Fig. 8 attenuates all frequencies outside of the band  $\omega_{\text{hp}} < \omega_{\text{HET}} < \omega_{\text{lp}}$ , where we are working in radians/s,  $\omega \equiv 2\pi F$ . There is a phase shift associated with the high-pass and low-pass filters which change the phase by  $\tan^{-1}(\omega_{\text{hp}}/\omega_{\text{HET}})$  and  $\tan^{-1}(\omega_{\text{HET}}/\omega_{\text{lp}})$  respectively.  $\omega_{\text{hp}}$  and  $\omega_{\text{lp}}$  are determined by resistance and capacitance values which will drift with temperature. Low drift thin-film resistors are readily available, but even good quality capacitors [10] will drift  $\sim 0.01\%$  per degree C.

The change in phase per change in capacitance can be predicted: Let  $u = \omega_{\text{hp}}/\omega_{\text{HET}}$ . A fractional increase in capacitance will cause an equal fraction decrease  $\Delta u/u$ , which will in turn cause a phase shift

$$\Delta\phi = u/(1+u^2) (\Delta u/u) \text{ radians.} \quad (3)$$

Example: if  $F_{\text{HET}}=100$  kHz, and the high-pass and low-pass frequencies are 50 kHz and 200 kHz respectively, so that for high-pass  $u=1/2$  and for low-pass  $u=2$ . A 0.01% change in capacitor values (as expected for a 1 degree C change) will cause a phase shift  $\Delta\phi = (0.5)/(1+(0.5)^2)(0.0001) = 4 \times 10^{-5}$  radians  $= 6.4 \times 10^{-6}$  cycles.

It should be remembered that an equal contribution *also* comes from the low-pass filter. Indeed, if there are  $N$  bandpass filters, the drift will be multiplied by  $2N$ . So for 4 bandpass filters, a 1 degree C change causes

$\Delta\phi=5.1\times 10^{-5}$  cycles. Doubling the frequency range to 25 to 400 kHz would reduce  $\Delta\phi$  to  $3\times 10^{-5}$  cycles.

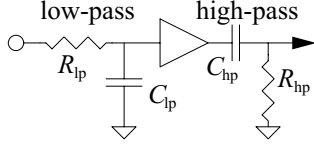


Fig. 8. Bandpass filter that allows through frequencies between  $\omega_p=(R_{lp}C_{lp})^{-1} > \omega > \omega_{hp}=(R_{hp}C_{hp})^{-1}$  radians/s. In practice, the buffer separating the low-pass and high-pass sections can be eliminated if  $R_{lp} \ll R_{hp}$ , (making it easy to modularise the bandpass filters).

#### 4. GLITCHES

Because of the small photodiode currents (typically  $<1$   $\mu$ A, for  $\sim 2$   $\mu$ W impinging on the p.d.) the total gain from the front-end to the zero-crossing detector must be high (a few  $\times 10^6$  V/A in the bandpass frequencies). This large gain increases system susceptibility to technical noise: electric motors, radio stations etc. (Photodetector shot noise is also present, but is not an issue at these power levels.)

Technical noise tends to be impulsive, and it is very difficult to prevent it from causing unwanted zero-crossings which are seen as jumps (glitches) in phase of an integer number of cycles, which in turn cause problems for system control loops and complicate data analysis.

The cure for glitches is

1. paying attention to the previously discussed “lessons learned” and
2. increasing the AC current signal out of the photodiode (increasing the laser power, achieving better fringe contrast).

In our experience, narrowing the bandpass filters, and/or adding more filter stages does not help much. If cures 1 and 2 don’t do the job, then phase-locked-loops can be used.

##### 4.1 Glitch removal with phase-locked-loops

The addition of a phase-locked loop (PLL) [11] is a potent cure for glitches. Conceptually, the PLL is variable, voltage controlled frequency oscillator (VCO) with a mechanism that makes it closely follow the frequency and phase of the square wave from the zero crossing detector. In principle, the phase of the PLL output oscillator is equal to the zero-crossing phase plus a constant offset, usually 90 degrees. Input glitches are ignored by the PLL oscillator, which supplies a clean square wave to the phasemeter.

In practice, the phase relationship between the PLL input and output drifts with temperature. For the

74HC4046 we see roughly  $2.5\times 10^{-4}$  cycles/C sensitivity. Further work should greatly improve this aspect of the circuit.

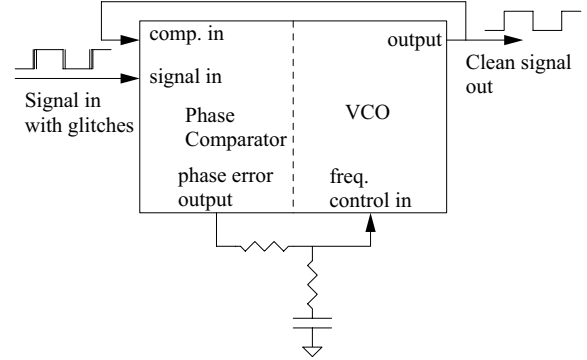


Fig. 9. Insertion of a PLL between the zero crossing detector and the phasemeter input, to remove glitches.

An additional benefit of the PLL technique is that it allows glitch-free measurement of low S/N signals, allowing much lower laser power. We are taking advantage of this in the JWST dilatometer where low sample heating, low incident power, are required.

#### 5. CYCLIC ERROR, CROSTALK

As previously mentioned, cross-talk between channels will cause a cyclic non-linearity in the measured phase. The approximate rms magnitude of this error is predicted [12] by the expression

$$\begin{aligned} \varepsilon(\phi) &= 2^{-1/2}(1/2\pi)(V_l/V_{pp}) \quad (4) \\ &\approx (1/9)(V_l/V_{pp}), \end{aligned}$$

in cycles, where  $V_l$  is the amplitude of the leakage signal at the zero-crossing detector input and  $V_{pp}$  is the amplitude of the “good” signal. A spectrum analyser may be used to measure the ratio  $V_l/V_{pp}$  where it will be typically expressed in dB.  $R_{dB} = -20\log_{10}(V_l/V_{pp})$ .

Example: a spectrum analyser monitoring the zero-crossing detector input shows that a “good” signal strength of 13 dBm and a leakage signal from the adjacent channel of -47 dBm. The 60 dB difference indicates that  $V_l/V_{pp}$  is  $10^{-3}$ , hence the rms cyclic error will be about  $10^{-4}$  cycles.

This level of leakage is typical of systems where ground loops, cabling, shielding and power supply distribution were not taken into consideration. Applying the “lessons learned” will help get the 80 dB inter-channel isolation needed for  $10^{-5}$  cycle accuracy.

#### 6. NEW POST-AMP DESIGN

A new signal-processing module (Figs 10, 11) incorporating all the “lessons learned” has been built

and is in use by the JWST dilatometer and TPF nulling testbeds. Features of the post-amp include:

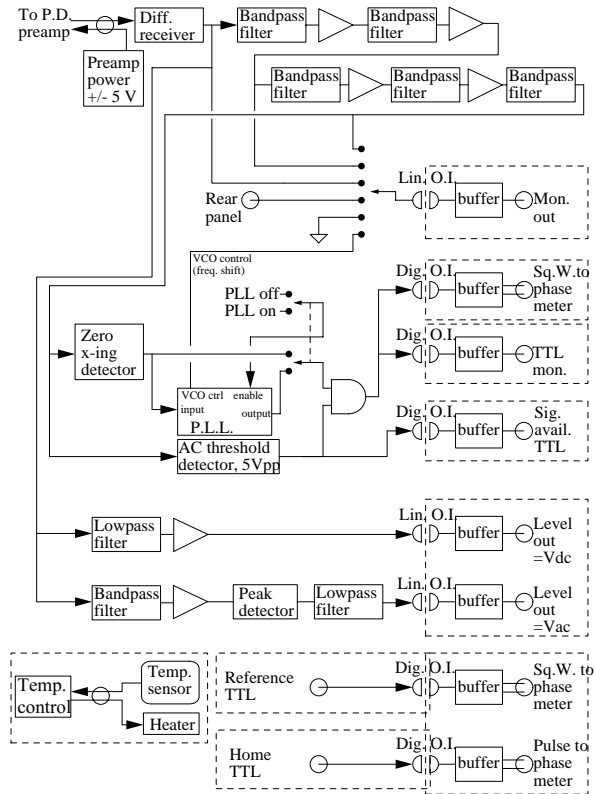


Fig. 10. Block diagram of JWST/TPF metrology post-amp. Dashed lines indicate boundaries of sections of the circuit that are isolated from each other, have separate floating grounds and independent power supplies to reduce cross-talk and to eliminate ground loops.

1. Incorporation of all the “lessons learned”.
2. Electronics temperature regulated to 0.1 C for long-term stability.
3. Modular bandpass filters for easy changes in  $F_{HET}$
4. Glitch removal using PLL circuits, user selectable.
5. All outputs optically isolated. No interconnected grounds.
6. Outputs including
  - a. heterodyne signal waveform,
  - b. fringe visibility (contrast) AC and DC components,
  - c. PLL feedback,
  - d. TTL and differential square wave output.
7. Isolated power supply for photodiode preamp.
8. Bias for low heat dissipation single transistor differential driver (Fig. 4), user selectable.
9. Isolated interfaces for phase meter reference clock and HOME (integer phase reset) signal.



Fig 11. Photo of JWST/TPF metrology post-amps. Top module is open, showing multiple power supplies (rear) and the constant temperature oven (front). The bottom module is a six-channel temperature controller maintaining the ovens at 30.0 C.

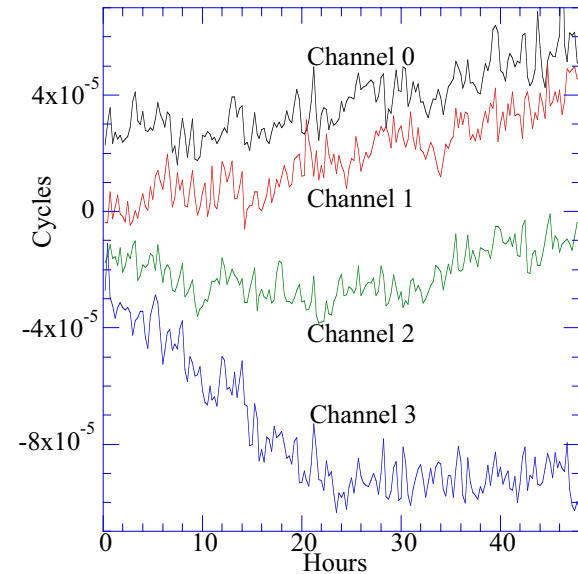


Fig. 12. Drift of JWST/TPF post-amps over forty-eight hours. Each point is 15 minutes of data, averaged.

## 7. POST-AMP RESULTS

The performance of the JWST/TPF post-amps is illustrated in Fig. 12, and summarized in Table 2.

To obtain the forty-eight stability plot, an Agilent 34401A signal generator, whose internal clock was locked to the phasemeter’s reference clock, fed 20 mV rms, 16 kHz sinusoids to four post-amps. To reduce the effect of digitization noise from the phasemeter, a small amount of noise was added to the sinusoids, enough to cause several LSB of phase noise at the phasemeter inputs. The phasemeters were operated

with 0.1 C temperature regulation and with the glitch removing phase-locked loops on. The worst performance is in channel 3, which exhibits an rms drift of  $2.2 \times 10^{-5}$  cycles. For the JWST dilatometer which uses a 532 nm laser, this translates to 5.9 pm rms.

To summarize, we have gained the ability to predictably achieve  $\sim 10^{-5}$  cycle linearity and repeatability phase measurements of 2 kHz to 200 kHz heterodyne signals. This capability is enabling development of metrology needed by the JWST, TPF and SIM missions.

Table 2. Performance of JWST/TF post-amps.

		Notes
Frequency range	2 kHz to 200 kHz.	Diagnostic waveform output limit < 50kHz
Noise	$2.2 \times 10^{-8}$ V/Hz <sup>1/2</sup>	Equivalent input noise.
Gain	1 to $2 \times 10^4$	
Filtering	5 bandpass	User defined
Phase locked-loop	Selectable on/off	Freq. and tracking user defined.
amplitude-to-phase coupling $d\phi/dR_A$	$< 2 \times 10^{-5}$ cycles	Example: 5% ampl. change causes $< 10^{-6}$ cycle phase shift
Thermal sensitivity	$\sim 2 \times 10^{-5}$ cycles/C	No temp. control, no PLL.
Thermal sensitivity	$\sim 2.5 \times 10^{-4}$ cycles/C	With PLL, no temp. control.
Temperature regulation	0.1 C	
Stability with temp. control	$\sim 2 \times 10^{-6}$ cycles	Expected, no PLL
Stability with temp. control	$\sim 2.5 \times 10^{-5}$ cycles/C	Expected, with PLL
Stability with temp. control	$< 2.2 \times 10^{-5}$ cycles	Measured, rms over 48 hours, with PLL.
Crosstalk	$\sim -90$ dB	Typical, well-shielded signal cables.

## 8. ACKNOWLEDGEMENTS

The authors wish to acknowledge the hard work of Raymond Savedra who implemented many of the circuits discussed here and of Dorian Valenzuela and Guadalupe Sanchez who fabricated the new post-amps. This research was carried out at the Jet Propulsion Laboratory, California Institute of Technology, under a contract with the National Aeronautics and Space Administration.

## 9. REFERENCES

1. *SIM, Taking the Measure of the Universe*, JPL publication 400-811 3/99 (Available online at [sim.jpl.nasa.gov/library/book.html](http://sim.jpl.nasa.gov/library/book.html))
2. *The Terrestrial Planet Finder (TPF): A NASA Origins Program to Search for Habitable Planets*, JPL publication 99-003 4/99 (Available online at [planetquest.jpl.nasa.gov/TPF/tpf\\_book/index.html](http://planetquest.jpl.nasa.gov/TPF/tpf_book/index.html))
3. Goullioud R., Wide Angle Astrometric Demonstration on the Micro-Arcsecond Metrology Testbed for the Space Interferometry Mission, *Proceedings of ICSO 2004, 5<sup>th</sup> International Conference on Space Optics* (this conference).
4. Halverson P.G. et al., Progress Towards Picometer Accuracy Laser Metrology for the Space Interferometry Mission – Update for ICSO 2004, *Proceedings of ICSO 2004, 5<sup>th</sup> International Conference on Space Optics* (this conference).
5. Martin S., A System Level Testbed for a Mid-infrared Beam Combiner for Terrestrial Planet Finder, to be published in *2004 IEEE Aerospace Conf.*, March 2004, Big Sky, Montana, IEEEAC paper #1266
6. Dudik M. et al., Precision Cryogenic Dilatometer for James Webb Space Telescope Materials Testing, *Fifteenth Symposium on Thermophysical Properties*, June 2003, Boulder Colorado, <http://symp15.nist.gov/pdf/p199.pdf>
7. Halverson P.G. et al., A Multichannel Averaging Phasemeter for Picometer Precision Laser Metrology, *Optical Engineering for Sensing and Nanotechnology (ICOSN '99)* conference, 16-18 June 1999, Yokohama, Japan, *Proceedings of the SPIE*, V.3740, pp 646-649
8. Horowitz P. and Hill W., *The Art of Electronics, 2nd Ed.*, page 77, figure. 2.28, Cambridge University Press, Cambridge, U.K., 1989.
9. *OPA227, OPA228, High Precision, Low Noise Operational Amplifiers*, Burr-Brown (now Texas Instruments) product data sheet.
10. *ECHS PPS Film Capacitor*, Panasonic data sheet.
11. *74HC4046A, High-Speed CMOS Logic Phase-Locked-Loop with VCO*, Fairchild (now Texas Instruments) product data sheet.
12. Halverson P.G. and Spero R.E., Signal Processing and Testing of Displacement Metrology Gauges with Picometre-scale Cyclic Nonlinearity, *Journal of Optics A: Pure and Applied Optics*, V.4, S304-S310, 2002.